Local quantum criticality in the two-dimensional dissipative quantum XY model

Lijun Zhu,[1] Yan Chen,[2,3] and Chandra M. Varma[1]
[1]*Department of Physics and Astronomy, University of California, Riverside, California 92521, USA*
[2]*Department of Physics and State Key Laboratory of Surface Physics, Fudan University, Shanghai 200433, China*
[3]*Collaborative Innovation Center of Advanced Microstructures, Nanjing 210093, China*
(Received 22 December 2014; published 22 May 2015)

We use quantum Monte Carlo simulations to calculate the phase diagram and the correlation functions for the quantum phase transitions in the two-dimensional dissipative quantum XY model with and without fourfold anisotropy. Without anisotropy, the model describes the superconductor-to-insulator transition in two-dimensional dirty superconductors. With anisotropy, the model represents the loop-current order observed in the underdoped cuprates and its fluctuations, as well as the fluctuations near the ordering vector in simple models of two-dimensional itinerant ferromagnets and itinerant antiferromagnets. These calculations test an analytic solution of the model which reexpressed it in terms of topological excitations: the vortices with interactions only in space but none in time, and warps with leading interactions only in time but none in space, as well as subleading interactions which are both space and time dependent. For parameters where the proliferation of warps dominates the phase transition, the critical fluctuations as functions of the deviation of the dissipation parameter α on the disordered side from its critical value α_c are scale invariant in imaginary time τ as the correlation length in time $\xi_\tau = \tau_c e^{[\alpha_c/(\alpha_c-\alpha)]^{1/2}}$ diverges, where τ_c is a short-time cutoff. On the other hand, the spatial correlations develop with a correlation length $\xi_x \approx \xi_0 \ln(\xi_\tau)$, with ξ_0 of the order of a lattice constant. The dynamic correlation exponent z is therefore ∞. The Monte Carlo calculations also directly show warps and vortices. Their densities and correlations across the various transitions in the model are calculated and related to those of the order-parameter correlations in the dissipative quantum XY model.

DOI: 10.1103/PhysRevB.91.205129 PACS number(s): 71.10.Hf, 05.30.Rt, 74.72.−h, 74.81.Fa

I. INTRODUCTION

The dissipative quantum XY model was introduced [1,2] to describe the observed quantum phase transition [3] in thin metallic films from a superconductor to insulator at a universal value of their normal-state resistance. In the past few years, the model has acquired applications in other physical contexts. The new physical contexts are the quantum-critical point of the loop-current order in cuprate superconductors [4–6], and the two-dimensional (2D) itinerant antiferromagnetic (AFM) quantum-critical point [7], which may be of relevance to Fe-based superconductors and some heavy-fermion compounds. It is also of course directly applicable to quantum critical points in 2D XY ferromagnets.

Electronic-fluctuation-induced superconductivity in cuprates, Fe-based superconductors, and in heavy-fermion superconductors always appears together with a normal state which does not obey the Fermi-liquid paradigm. For cuprates, the properties of the normal state, sometimes called the strange metal phase, could be phenomenologically described as a marginal Fermi liquid (MFL) [8], in which the coupling of electrons is to quantum-critical fluctuations which are local in space and power law in time. Such critical fluctuations violate the paradigm of classical dynamical critical fluctuations [9] or their simple quantum analogs [10–12]. The anomalous normal-state properties have been associated with quantum criticality of an order competing with superconductivity. Thermodynamic and transport properties near the antiferromagnetic quantum-critical point of some heavy-fermion compounds [13] and at least some of the Fe-based superconductors near their antiferromagnetic quantum-critical point are remarkably similar to these in the cuprates [14,15]. The quantum-critical fluctuations of one of the heavy-fermion compounds, measured by neutron scattering [16–18], has also been fitted to a form of local-critical fluctuations [19]. All these problems share the property that they are highly anisotropic so that the fluctuation problem may be regarded as two dimensional in space. The microscopic physics in these problems is of course quite different. The universality class of local quantum criticality appears to encompass diverse physical systems.

The dissipative quantum XY model is a quantum generalization of the classical 2D XY model. The latter can be solved by integrating over the spin-wave variables to cast the model in terms of topological excitations, the vortices, which are responsible for the Kosterlitz-Thouless (KT) transition: vortices occur as bound pairs of zero net vorticity at low temperatures while individual vortices proliferate in the high-temperature disordered phase [20,21]. The dissipative quantum XY model has two additional features: (1) the kinetic energy of the fixed length 2D rotors, and (2) dissipation of the (gradient of the) angular degrees of freedom. When dissipation is unimportant, the quantum model has been shown to have a quantum phase transition in the universality class of classical three-dimensional (3D) XY model (with dynamical critical exponent $z = 1$) [22] for the ratio of the kinetic energy parameter to the spatial coupling of the rotors above a critical value [23]. When dissipation is important, the problem may be usefully reparametrized in terms of new degrees of freedom, which are two orthogonal sets of topological excitations, the vortices and the warps [6] (see also Sec. II B). It is claimed that when the quantum phase transitions in the model are governed by proliferation of warps, the transitions are of the local critical type and the critical fluctuations are of the form phenomenologically proposed for MFL [8]. It is important to have an unambiguous check of this solution of the model and its variants by other methods. The method used here is to simulate the model with the quantum Monte Carlo method.

In a set of Monte Carlo calculations already done on the model [24], a rich phase diagram of the model was discovered. However, the correlations of the order parameter in some important regions were not studied, nor were the properties of the model related to the topological excitations proposed [6]. The results for all the quantities calculated here which were also calculated earlier [24] are identical. In this work, we calculate the correlation functions and relate them to those of the topological excitations which can be identified explicitly in the Monte Carlo calculations. We show that for transitions driven by warps, the order-parameter fluctuations at the critical point are scale invariant in imaginary time τ, and calculate the behavior of the correlation functions as the critical point is approached. A result beyond those derived analytically is that the spatial correlations are consistent with a length scale ξ_x which grows only logarithmically with the temporal length scale ξ_τ. This is consistent with a dynamical exponent $z \to \infty$, making it a model in which local quantum criticality is explicitly proven.

We do not study, in this paper, the $z = 1$ transition where the kinetic energy rather than the dissipation drives the transition, nor the passage between these two distinct types of transitions. That is clearly interesting and important but is reserved for future work.

This paper is organized as follows. We introduce the model and the details of quantum Monte Carlo method in Sec. II. In Sec. II B, we explain how we identify the warps and vortices in the calculations. We show the obtained phase diagram and summarize the properties of three distinct phases: the disordered, quasiordered, and ordered phases, in Sec. III. In Secs. IV, V, and VI, we show the calculated critical fluctuations of the order parameter at the transitions between them, and their relation to the change in density and correlations of warps and vortices across the transitions. We focus especially on the transition from the disordered phase to the ordered phase (Sec. VI), and explicitly show that the fluctuations have a temporal correlation length exponentially larger than the spatial correlation length. In Sec. VII, we discuss the effect of a fourfold anisotropic field, relevant to cuprates and the antiferromagnets. Our conclusion and the directions for future analytical calculations are presented in Sec. VIII.

II. MODEL AND METHOD

A. (2+1)D quantum dissipative XY model

The action of the (2+1)D quantum dissipative anisotropic XY model is [24]

$$\begin{aligned} S = &-K_0 \sum_{\langle \mathbf{x},\mathbf{x}'\rangle} \int_0^\beta d\tau \, \cos(\theta_{\mathbf{x},\tau} - \theta_{\mathbf{x}',\tau}) \\ &+ \frac{1}{2E_c} \sum_{\mathbf{x}} \int_0^\beta d\tau \left(\frac{d\theta_{\mathbf{x}}}{d\tau}\right)^2 \\ &+ \frac{\alpha}{2} \sum_{\langle \mathbf{x},\mathbf{x}'\rangle} \int d\tau \, d\tau' \frac{\pi^2}{\beta^2} \frac{[(\theta_{\mathbf{x},\tau} - \theta_{\mathbf{x}',\tau}) - (\theta_{\mathbf{x},\tau'} - \theta_{\mathbf{x}',\tau'})]^2}{\sin^2\left(\frac{\pi|\tau-\tau'|}{\beta}\right)} \\ &- h_4^0 \sum_{\mathbf{x}} \int d\tau \, \cos(4\theta_{\mathbf{x},\tau}), \end{aligned} \tag{1}$$

where $\mathbf{x}$ labels the coordinates of a lattice site in 2D spatial dimension and τ labels an imaginary time in extra temporal dimension. $\tau \in [0,\beta]$, where β is the inverse of temperature $1/(k_B T)$. $\theta_{\mathbf{x},\tau}$ is the angle of the planar spin. $\langle \mathbf{x},\mathbf{x}'\rangle$ denotes nearest neighbors. The first term is the spatial coupling term as in the classical XY model. The second term is the kinetic energy where the charging energy E_c serves as the moment of inertia. The third term describes quantum dissipations of the Ohmic or Caldera-Leggett type [25]. The physical origin of such a term in the context of superconductor-insulator transitions [1,2], and in the context of loop-current order in cuprates [6], has been discussed. In the former case, the dimensionless dissipation strength α is the ratio of the quantum of resistance $R_Q = h/(4e^2)$ to the shunt resistance R_s: $\alpha = (1/4\pi^2)R_Q/R_s$ [1,2]. A dissipation-driven phase transition occurs typically at $R_Q \sim R_s$, or $\alpha \sim 0.025$. In the latter case, we note that the symmetry of the loop-current order is described by the Ashkin-Teller (AT) model with four discrete directions of the θ variables (or two Ising variables $\sigma^{x,y}$). We simulate the Ashkin-Teller model by imposing a strong fourfold anisotropic field h_4^0 (the fourth term). We recall that the anisotropy is marginally irrelevant in the classical 2D XY model [26]. Strictly speaking, we should also add a term with interactions $\propto \cos[2(\theta_{\mathbf{x},\tau} - \theta_{\mathbf{x}',\tau})]$ to represent the Ashkin-Teller model completely. Such a term has been shown to be irrelevant in the analytic calculations [6] in the fluctuation regime. We have verified this assertion in the Monte Carlo calculations.

In numerical simulations, we choose a 2D square lattice with $N \times N$ lattice sites. Periodic boundary conditions are imposed along both x and y directions. We further discretize the imaginary-time axis $[0,\beta]$ into N_τ slices. In this discretized (2+1)D lattice, the action can be rewritten as

$$\begin{aligned} S = &-K \sum_{\langle \mathbf{x},\mathbf{x}'\rangle,\tau} \cos(\Delta\theta_{\mathbf{x},\mathbf{x}',\tau}) + \frac{K_\tau}{2} \sum_{\mathbf{x},\tau} (\theta_{\mathbf{x},\tau} - \theta_{\mathbf{x},\tau-1})^2 \\ &+ \frac{\alpha}{2} \sum_{\langle \mathbf{x},\mathbf{x}'\rangle,\tau,\tau'} \frac{\pi^2}{N_\tau^2} \frac{[\Delta\theta_{\mathbf{x},\mathbf{x}',\tau} - \Delta\theta_{\mathbf{x},\mathbf{x}',\tau'}]^2}{\sin^2\left(\frac{\pi|\tau-\tau'|}{N_\tau}\right)} \\ &- h_4 \sum_{\mathbf{x},\tau} \cos(4\theta_{\mathbf{x},\tau}), \end{aligned} \tag{2}$$

where $K_\tau \equiv 1/(E_C \Delta\tau)$, $K \equiv K_0 \Delta\tau$, $h_4 = h_4^0 \Delta\tau$, and $\Delta\tau = \beta/N_\tau$. We choose K, K_τ, α, and h_4 as independent dimensionless variables, and tune them separately. In other words, we consider the variables in units of the physical ultraviolet cutoff $\Delta\tau$ which is fixed. In this representation, the temperature is controlled by N_τ^{-1}. The calculations are asymptotically correct for the quantum problem when $1/\beta = T \to 0$ or $N_\tau \to \infty$. This requires in practice that we ensure that the results converge in the range of N_τ actually studied.

B. Analytic transformation of the model: Warps, vortices etc.

It is useful to briefly review the analytic solution of the model in order to understand several aspects of the Monte Carlo results including the physics of the three different phases found in Ref. [24] and the mechanism for the relative spatial locality of the fluctuations. In Ref. [6], it is shown that after making a Villain transformation [27] and integrating over the small oscillations or spin waves, the action is expressed in

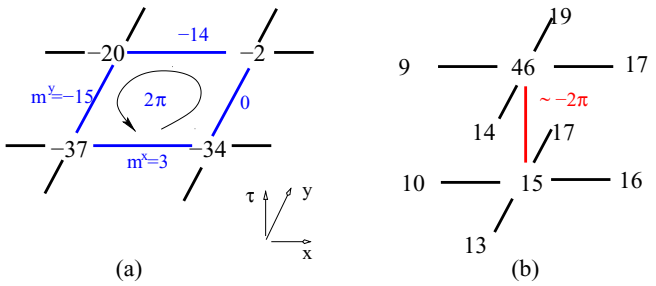

FIG. 1. (Color online) Examples of vortex (a) and warp (b) excitations in numeric simulation. The numbers at the lattice points (in space or time) are the θ's in units of $2\pi/32$ and are noncompact variables. The numbers in the links are the velocity fields, i.e., the difference of θ's that a link connects. (a) For the plaquette shown, $(\nabla \times \mathbf{m})_{i,j,\tau}$ is 32, or 2π, showing a vortex. In (b), the change of $(\hat{\nabla} \cdot \mathbf{m})_{i,j,\tau}$ for two neighboring time slices is close to -2π, showing an antiwarp.

terms of link variables which are differences of θ's at nearest-neighbor sites, as shown in Fig. 1:

$$m_{\mathbf{x},\mathbf{x}'}(\tau,\tau') \equiv \theta(\mathbf{x},\tau) - \theta(\mathbf{x}',\tau'). \tag{3}$$

Further,

$$\mathbf{m} = \mathbf{m}_\ell + \mathbf{m}_t, \tag{4}$$

where $\mathbf{m}_\ell$, is the longitudinal (or curl-free) part and $\mathbf{m}_t$ is the transverse (or divergence-free) part. The appearance of $\mathbf{m}_\ell$ is a distinct feature of the quantum dissipative XY model. Now, define

$$\nabla \times \mathbf{m}_t(\mathbf{x},\tau) = \rho_v(\mathbf{x},\tau)\hat{\mathbf{z}}, \tag{5}$$

so that $\rho_v(\mathbf{x},\tau)$ is the charge of the vortex at $(\mathbf{x},\tau)$, and

$$\frac{\partial \hat{\nabla} \cdot \mathbf{m}_\ell(\mathbf{x},\tau)}{\partial \tau} = \rho_w(\mathbf{x},\tau). \tag{6}$$

$\rho_w(\mathbf{x},\tau)$ is called the "warp" at $(\mathbf{x},\tau)$.

Although a continuum description is being used for simplicity of writing, it is important to do the calculation so that the discrete nature of the ρ_v, ρ_w fields is always obeyed. In the numerical implementation of (2+1)D discrete lattice, given the two bonds per site $(\mathbf{x})$, one may construct a vector field $\mathbf{m}_{\mathbf{x},\tau}$, whose components are the two directed link variables in the Cartesian directions:

$$\begin{aligned} m^x_{i,j,\tau} &= \theta_{i+1,j,\tau} - \theta_{i,j,\tau}, \\ m^y_{i,j,\tau} &= \theta_{i,j+1,\tau} - \theta_{i,j,\tau}, \end{aligned} \tag{7}$$

as shown in Fig. 1. Here, $\mathbf{x} = (i,j)$.

In terms of the vortex and warp densities, the action of the model was shown to be [6]

$$S = T\sum_{\mathbf{k},\omega_n}\left[\frac{K}{k^2}|\rho_v(\mathbf{k},\omega_n)|^2 - \frac{\alpha}{|\omega_n|}|\rho_w(\mathbf{k},\omega_n)|^2 - G(\mathbf{k},\omega_n)\left(KK_\tau - \alpha K_\tau|\omega_n| - \alpha^2k^2\right)|\rho_w(\mathbf{k},\omega_n)|^2\right], \tag{8}$$

where

$$G(\mathbf{k},\omega_n) = \frac{1}{Kk^2 + K_\tau\omega_n^2 + \alpha|\omega_n|k^2}. \tag{9}$$

The first term is the action of the *classical* vortices interacting with each other through logarithmic interactions in space but the interactions are local in time. The second term describes the warps interacting logarithmically in time but locally in space. In the third term, the terms proportional to α may be dropped in both the numerator and the denominator. Then, this is just the action for a Coulomb field, which if present alone is known [28] not to cause a transition and is therefore marginally irrelevant in the present problem. The warp and the vortex variables in the first two terms are orthogonal. With just these two terms alone, the problem is exactly soluble. If the first term dominates, one expects a transition of the class of the classical Kosterlitz-Thouless transition through binding of vortex-antivortex pairs in space, but there is nothing to order the vortices with respect to each other in time. If the second term dominates, there is a quantum transition to a phase with binding of warp-antiwarp pairs in time but nothing to order them with respect to each other in space. Given the ordering driven by either the density of isolated vortices or of isolated warps $\to 0$, the flow from one to the other is determined by the third term leading to possible ordering at $T = 0$ both in time and space. The phase diagram calculated from the starting model (1), shown in Fig. 2, is consistent with these expectations from the transformed model (8). It should be noted that vortices and warps enter asymmetrically in this model; although a spatially ordered phase at a given time slice with no ordering between time slices is expected for a range of parameters, no phase with time order but no spatial order is expected.

The transformation to the topological model relies on a finite dissipation coefficient α. One cannot take the limit $\alpha \to 0$ and expect to get back the properties of the (2+1)D quantum XY model without dissipation, which should have a quantum

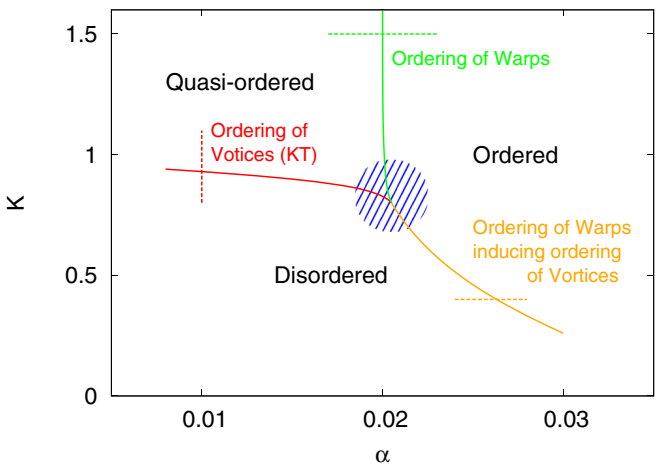

FIG. 2. (Color online) Phase diagram for the quantum dissipative XY model in α-K plane. Here, $K_\tau = 0.01$. The transition points are determined from the nonanalyticity in various static properties with a system size $N = 50$ and $N_\tau = 200$ (the transition points for infinite systems can be determined by a finite-size analysis). The area where the lines join (blue shaded area) has not been explored thoroughly enough to precisely determine how the phase boundaries meet. The dashed lines show the sweep of parameters presented in the following sections for the study of correlations across the three types of transitions. The phase diagram is obtained by several such sweeps across each transition.

transition of the class of 3D classical XY model. An important unsolved question is at what value of α do the transitions of the starting model (1) change from that class to those studied here.

It was derived in Ref. [6] based on (8) that when the ordering is driven through warps, the fluctuations of the order parameter at the critical point have $1/\tau$ correlations, in time at the critical point [which on appropriate thermal Fourier transformation gives a spectral function $\tanh(\omega/2T)$]. This result will be verified in the Monte Carlo calculations in the following on the original model.

C. Quantum Monte Carlo simulations

We follow the numerical procedure as in Ref. [24] for the Monte Carlo simulations. To speed up the simulation, we choose $\theta_{\mathbf{x},\tau}$ to be a discrete variable $n2\pi/32$ (n an integer), rather than a continuous variable. Adding more states does not affect the results, as found in Ref. [24] and confirmed in our calculation. The system size typically chosen is $N = 50$ and $N_\tau = 200$, which are found to be adequate for the parameter ranges not too close to the critical points. Other system sizes are also used in scaling analysis calculations.

We start from a random configuration of $\{\theta_{\mathbf{x},\tau}\}$. To update the configuration, we sequentially sweep the lattice sites to update locally $\theta_{\mathbf{x},\tau}$ to $\theta_{\mathbf{x},\tau} + \theta'$, where θ' is a random angle between -2π and 2π. We make measurements of the physical quantities of interest after 10 sweeps. We also employ parallel tempering technique to speed up the relaxation. The acceptance rate for this local update ranges from 46% (disordered state) to 16% (ordered state) in the range of parameters being calculated. We typically choose $O(10^4)$ warm up sweeps and $O(10^6)$ measurements in our Monte Carlo simulations. For large enough measurements, the desired thermodynamic averages and correlation functions are well approximated.

The following quantities are calculated to characterize the different phases and the transitions between them.

Action susceptibility. The action susceptibility is defined as

$$\chi_S = \frac{1}{N^2 N_\tau}(\langle S^2\rangle - \langle S\rangle^2), \tag{10}$$

where $\langle\ldots\rangle$ denotes averaging over the $O(10^6)$ Monte Carlo measurements. In classical systems, as $S = \beta H$, χ_S is related to the specific heat $\chi_S = C_V/k_B$. At $T \to 0$, it is a measure of zero-point fluctuations which are expected to be singular at the critical point due to the degeneracy in the spectra.

Helicity modulus. The helicity modulus or spatial stiffness is defined from the change of energy resulting from the slow twist of spins along the spatial direction, or

$$\Upsilon_x = \frac{1}{N^2 N_\tau}\left\langle \sum_{\langle \mathbf{x},\mathbf{x}'\rangle}\sum_{\tau}\cos(\Delta\theta_{\mathbf{x},\mathbf{x}',\tau})\right\rangle - \frac{K}{N^2 N_\tau}\left\langle\left(\sum_{\langle \mathbf{x},\mathbf{x}'\rangle}\sum_{\tau}\sin(\Delta\theta_{\mathbf{x},\mathbf{x}',\tau})\right)^2\right\rangle. \tag{11}$$

In the disordered state, the two terms have comparable contributions and $\Upsilon_x \to 0$. In an ordered phase, the second term vanishes while Υ_x becomes finite.

Order parameter. For XY spins, the order parameter $\mathbf{M}(\mathbf{x},\tau) = (\cos\theta_{\mathbf{x},\tau}, \sin\theta_{\mathbf{x},\tau})$. Its modulus, the magnetization in the plane, is defined as

$$M = \frac{1}{N^2 N_\tau}\left\langle\left|\sum_{\mathbf{x},\tau} e^{i\theta_{\mathbf{x},\tau}}\right|\right\rangle. \tag{12}$$

In the classical 2D XY model, the ordered phase has a quasi-long-range order, where $M \sim (1/N)^{1/(8\pi K)}$ vanishes for $N \to \infty$. A question which we will be able to answer is whether there is a finite magnetization in the infinite-size limit for the quantum dissipative XY model. We also found it illuminating to calculate M_{2D}, the magnitude of magnetization in the planes at a given time τ and then average it over the τ. This is equivalent to finding the Kosterlitz-Thouless order parameter at each time slice and then averaging over the time slices:

$$M_{2D} = \frac{1}{N^2 N_\tau}\left\langle\sum_{\tau}\left|\sum_{\mathbf{x}} e^{i\theta_{\mathbf{x},\tau}}\right|\right\rangle. \tag{13}$$

By definition, $M \le M_{2D}$. Also, $M = M_{2D} \neq 0$ (for $N \to \infty$) only if there is perfect long-range order across time as well as space.

Correlation function of the order parameter. The principal results for the quantum-critical fluctuations are given by the order-parameter correlation functions

$$G_\theta(\mathbf{x},\tau) = \frac{1}{N^2 N_\tau}\sum_{\mathbf{x}',\tau'}\langle e^{i(\theta_{\mathbf{x}'+\mathbf{x},\tau'+\tau} - \theta_{\mathbf{x}',\tau'})}\rangle. \tag{14}$$

$G_\theta(\mathbf{x}\to\infty, \tau\to\infty) \to M^2$ while $G_\theta(\mathbf{x}\to\infty, \tau = 0) \to M_{2D}^2$. In Ref. [24], mean-square displacements in time $W^2_{\Delta\theta}$ are shown, which we have reproduced. These can also be obtained from the second moment of the above correlation function at $\mathbf{x} = 0$.

Vortices and warps: Densities and self-/mutual correlations. The curl of the vector field $\mathbf{m}$ can be calculated numerically from the four link variables of a plaquette,

$$\rho_v(\mathbf{x},\tau) = \frac{1}{2\pi}(\nabla\times\mathbf{m})_{i,j,\tau} = \left(m^x_{i,j,\tau} + m^y_{i+1,j,\tau} - m^x_{i+1,j+1,\tau} - m^y_{i,j+1,\tau}\right)/(2\pi), \tag{15}$$

where we restrict $m^{x,y}$ to be within $(-\pi,\pi)$ by adding or subtracting $n2\pi$. If $(\nabla\times\mathbf{m})_{i,j,\tau} = \pm 2\pi$, we identify a vortex/antivortex, or $\rho_v(\mathbf{x},\tau) = \pm 1$. Similarly, the divergence of the vector field can be calculated from four links connected to the site

$$(\hat{\nabla}\cdot\mathbf{m})_{i,j,\tau} = \left(m^x_{i,j,\tau} - m^x_{i-1,j,\tau} + m^y_{i,j,\tau} - m^y_{i,j-1,\tau}\right)/4. \tag{16}$$

We therefore use the following criterion to identify a warp (antiwarp) charge:

$$\rho_w(\mathbf{x},\tau) = 1, \text{ if } (\hat{\nabla}\cdot\mathbf{m})_{i,j,\tau+1} - (\hat{\nabla}\cdot\mathbf{m})_{i,j,\tau} > 2\pi - \delta\theta,$$
$$\rho_w(\mathbf{x},\tau) = -1, \text{ if } (\hat{\nabla}\cdot\mathbf{m})_{i,j,\tau+1} - (\hat{\nabla}\cdot\mathbf{m})_{i,j,\tau} < -2\pi + \delta\theta, \tag{17}$$

TABLE I. Characteristic properties of three phases of the dissipative XY model. Definitions of these quantities are provided in Sec. II C.

Quantity	Disordered	Quasiordered	Ordered
M	0	Decreases $\to 0$ for $N \to \infty$	Finite
ρ_v	O(1)	$\ll 1$	$\ll 1$
$G_v(x)$	Exponential	Power law	Power law
Υ_x	0	Finite, jump at transition	Finite, no jump at transition
ρ_w	O(1)	O(1)	$\ll 1$
$G_w(\tau)$	$1/\tau^2$	$1/\tau^2$	$1/\tau^\alpha (\alpha > 2)$
$G_\theta(x,0)$	Exponential	Quasi-long range	Long range
$G_\theta(0,\tau)$	Exponential	Exponential	Long range

where $\delta\theta \ll 2\pi$ to accommodate small-angle changes due to spin waves. Examples of vortices and warps are also shown in Fig. 1.

After identifying the vortex and warp charges $\rho_{v,w}(\mathbf{x},\tau)$ in the system, we can calculate their densities

$$\rho_{v,w} = \frac{1}{N^2 N_\tau} \sum_{\mathbf{x},\tau} \langle |\rho_{v,w}(\mathbf{x},\tau)| \rangle, \tag{18}$$

as well as their correlation functions

$$G_{v,w}(\mathbf{x},\tau) = \frac{1}{N^2 N_\tau} \sum_{\mathbf{x}',\tau'} \langle \rho_{v,w}(\mathbf{x}'+\mathbf{x},\tau'+\tau)\rho_{v,w}(\mathbf{x}',\tau') \rangle. \tag{19}$$

Charge neutrality for both vortices and warps should be preserved. We verify this by calculating the net density $\delta\rho_{v,w} = [\sum_{\mathbf{x},\tau} \langle \rho_{v,w}(\mathbf{x},\tau) \rangle]/(N^2 N_\tau)$, and find that, in practice, $|\delta\rho_v|/\rho_v < 10^{-5}$ and $|\delta\rho_w|/\rho_w < 10^{-2}$. To capture the correlations between warps and vortices, we also calculate

$$G_{vw} = \frac{1}{N^2 N_\tau} \sum_{\mathbf{x},\tau} \langle |\rho_v(\mathbf{x},\tau)\rho_w(\mathbf{x},\tau)| \rangle, \tag{20}$$

i.e., the probability to find vortices in the vicinity of a warp and vice versa. If warps and vortices are not correlated, we expect $G_{vw} = \rho_v \rho_w$.

For the spatial dependence of various correlation functions $G(\mathbf{x},\tau)$ where $\mathbf{x} = (x,y)$, we in practice only calculate the correlations along the x-axis $G(x,\tau)$ by setting $y = 0$, due to the symmetries along x and y axes.

III. SUMMARY OF THE PHASE DIAGRAM

We first study the dissipative quantum XY model [cf. Eq. (2)] without the fourfold anisotropic field h_4, whose effect is addressed in Sec. VII. We focus on the transitions driven by dissipations, for which a small kinetic energy parameter K_τ is chosen. The phase diagram in α-K plane with fixed $K_\tau = 0.01$ is given in Fig. 2. It is similar to the $K_\tau = 0.002$ phase diagram obtained in Ref. [24]. Here, three distinct phases are identified: a "disordered" phase, a "quasiordered" phase, and an "ordered" phase (named as NOR, CSC, and FSC phases, respectively, in Ref. [24]). Their properties are summarized in Table I. The disordered phase has short-ranged correlations in both the spatial and temporal directions. The quasiordered phase, while also having short-ranged temporal correlations, has a quasi-long-range order in 2D spatial plane (for each time slice), consistent with KT spatial order. M_{2D} is finite and falls off slowly for large N, as shown in Fig. 3. The order parameter M follows M_{2D} asymptotically for $N \gg N_\tau$ while $M \to 0$ for $N \ll N_\tau$. The ordered phase has long-range order in both spatial and temporal directions, where M goes to a finite value as $N, N_\tau \to \infty$.

The transition from the disordered to the quasiordered phase can be achieved by increasing K at small α. As the temporal correlations remain relatively unchanged across the transition, the transition is characterized by the spatial ordering as in the KT transition, due to binding of vortex of antivortex pairs. The quasiordered phase is a phase in which K is effectively ∞, and there is little fluctuation of phase difference in the spatial bonds. Then, we have a one-dimensional problem in the time direction, which for small enough α is disordered. For increasing α, the system also orders in time, leading to a transition from the quasiordered to the ordered phase. For small K, there is a direct phase transition from the disordered to the ordered phase. This is in general in accord with the discussion in the previous paragraph based on the properties expected for the

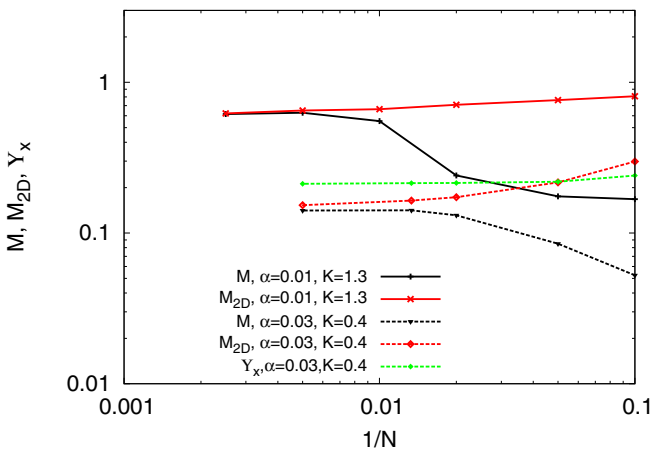

FIG. 3. (Color online) The spatial size dependence of M_{2D} and M in the quasiordered (top two curves) and ordered phases (bottom two curves). Also shown is Υ_x in the ordered phase. The parameters chosen for the quasiordered phase are $K_\tau = 0.01, \alpha = 0.01, K = 1.3$, and $N_\tau = 20$, while for the ordered phase, $K_\tau = 0.01$, $\alpha = 0.03$, $K = 0.4$, and $N_\tau = 100$. The slow decrease of the topmost curve (M_{2D}) is just the finite-size scaling to 0 at $N \to \infty$ in the Kosterlitz-Thouless phase [29], which M asymptotically joins. Their behaviors are different in the ordered phase, where asymptotically they are both consistent with a finite value at $N \to \infty$. The difference in Υ_x across the disordered to quasiordered and across the disordered to ordered phases is discussed in the text.

topological model of Eq. (8). We will show that the transition from the quasiordered to the ordered phase (in Sec. V) as well as that from the disordered to the ordered phase (in Sec. VI) occur primarily through freezing of warps. In the second transition, the vortices freeze as an accompaniment to the freezing of warps, in a manner distinct from that at the KT transition.

IV. TRANSITION FROM THE DISORDERED TO THE QUASIORDERED PHASE

The transition from the disordered to the quasiordered phase is studied by fixing $\alpha = 0.01$ and varying K. The static properties are shown in Fig. 4. We find that above a critical value K_c, which weakly depends on α, the spatial magnetization M_{2D} becomes finite. As shown in Fig. 3, M_{2D} decreases slowly when N increases. As discussed later, this decrease is consistent with the logarithmic decrease found in earlier calculations [29]. $M \to M_{2D}$ when $N_\tau \ll N$ and $M \to 0$ when $N_\tau \gg N$. The difference between M and M_{2D} is also reflected in the order-parameter correlations in the time direction, which shows oscillatory features at long times (not shown). This phase has only quasi-long-range (power-law) spatial order. As shown in Ref. [24], the helicity modulus Υ_x becomes finite in the quasiordered phase. Finite-size scaling of the helicity modulus Υ_x shows a Nelson-Kosterlitz [30] jump at K_c. This is related to the vortex density seen in Fig. 4, which decreases with increasing K, and changes slope at K_c. These are consistent with KT transition in the classical 2D XY model. Meanwhile, we find that in the temporal direction, all quantities remain relatively unchanged from those in the disordered phase. The vortex-warp correlation $G_{vw} \approx \rho_v \rho_w$, indicating vortices and warps are not correlated, in either the disordered or the quasiordered phase.

We also plot the correlation functions of warps and vortices in Fig. 4. For the equal-time vortex correlation $G_v(x,\tau = 0)$, $G_v(0,0) = \rho_v > 0$ (not shown due to the logarithmic scale) while $G_v(x \neq 0,0) < 0$, reflecting that the vortex-antivortex correlations dominate at long distance. When K increases, $-G_v(x,0)$ changes from an exponential decay in the disordered phase to a power-law decay in quasiordered phase. These are consistent with the KT transition as well. The warp correlation along temporal direction at the spatial site $G_w(0,\tau)$

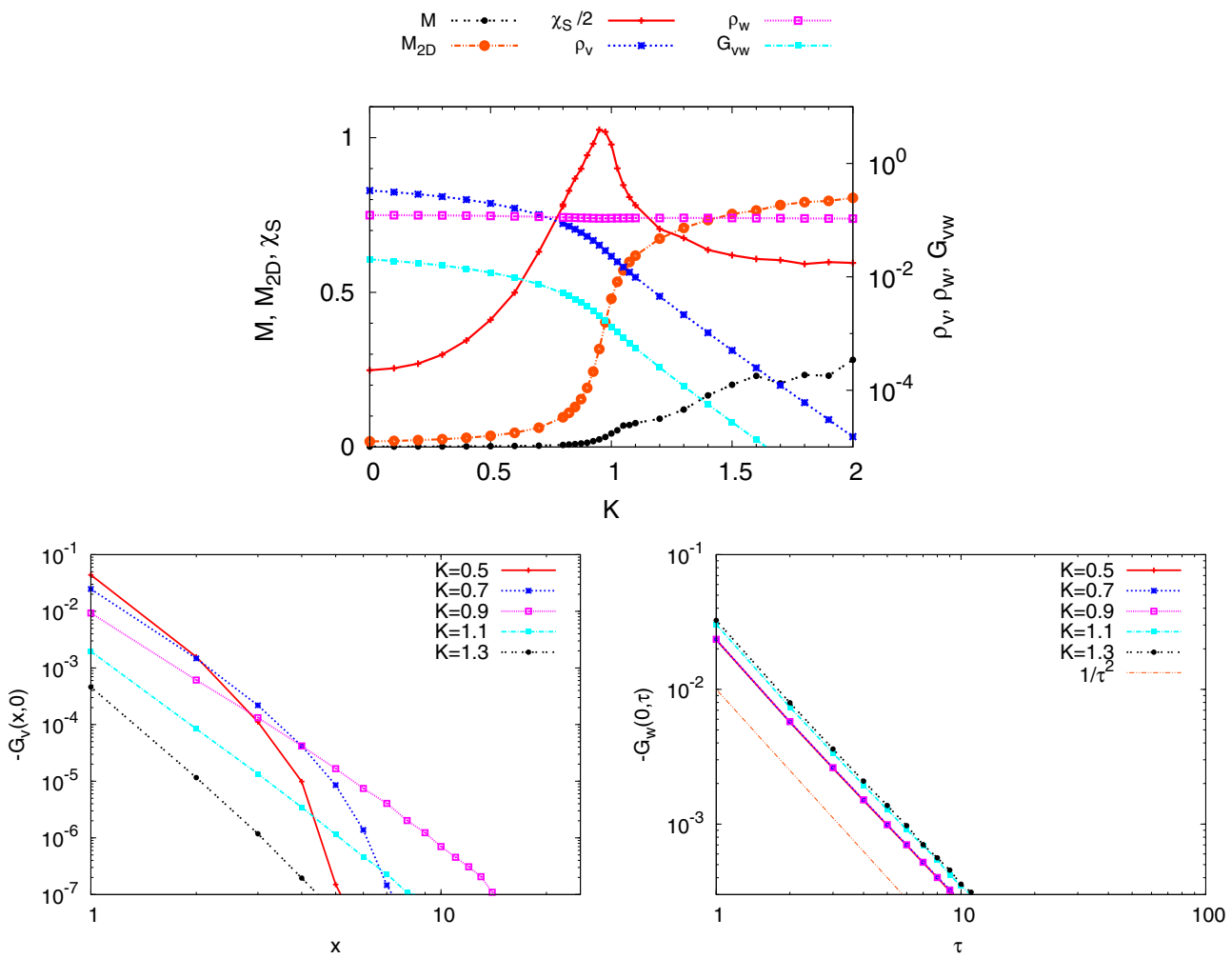

FIG. 4. (Color online) Static properties (top panel), vortex and warp correlation functions (bottom panels) of transition from the disordered to the quasiordered phase. Here, $K_\tau = 0.01$, $\alpha = 0.01$, and K is varied. The results shown are for $N = 50$ and $N_\tau = 200$. Note that some quantities are scaled to fit in the figure. The vortex density changes rapidly below the transition while the warp density remains smooth. Other aspects of the transition and of the quasiordered phase are discussed in the text.

also satisfies $G_w(0,0) = \rho_w > 0$ and $G_w(0,\tau \neq 0) < 0$. In this transition, it remains unchanged in asymptotic form $\propto 1/\tau^2$.

V. TRANSITION FROM THE QUASIORDERED TO THE ORDERED PHASE

We choose a suitable K and tune the transition from the quasiordered phase to the ordered phase by increasing the dissipation strength α. Various static properties as functions of α and correlation functions for selected α's are shown in Fig. 5. The peak in the action susceptibility χ_S implies a phase transition at $\alpha_c \approx 0.02$. We find that properties characterizing spatial orders, such as M_{2D}, ρ_v, and Υ_x, have small nonanalytic changes, as already discovered in Ref. [24]. The significant changes are properties characterizing temporal order. The asymptotic behavior of the warp density is similar to that of vortex density at KT transition: it changes slope at α_c and decreases exponentially as α further increases. M keeps increasing and saturates to M_{2D} at $\alpha \gg \alpha_c$ (at large system sizes). The warp correlation functions decay faster for larger α, changing from $1/\tau^2$ in the quasiordered phase to $1/\tau^a$ ($a \sim 3$ for $\alpha = 0.023$ in the figure) in the ordered phase. This indicates that warps and antiwarps, which are free in the quasiordered phase, also are bound in the ordered phase. Near α_c, a slower decay at large times is observed. As shown in the figure, it can be fitted as $1/\tau$. This is in agreement with the analytical analysis [6]. While the vortex-warp correlation $G_{vw} \sim \rho_v \rho_w$ in the quasiordered phase, we find $G_{vw} > \rho_v \rho_w$ in the ordered phase, and their difference increases when α is further increased from α_c. This implies that vortices and warps are correlated inside the ordered phase.

VI. TRANSITION FROM THE DISORDERED TO THE ORDERED PHASE

This is the part of the problem which we shall discuss most thoroughly. We show results for a suitable value $K = 0.4$ and tune α across the transition at $\alpha = \alpha_c(K)$. Similar results have been obtained for other values of these parameters across the transition, keeping $K_\tau = 0.01$ fixed at this low value. Note the fine scale on which α is varied compared to K in Fig. 2 to tune across the transition.

A. Static properties and correlations

The static properties shown in Fig. 6 are all nonanalytic near $\alpha_c \approx 0.0260$. We estimate an uncertainty of ± 0.0002

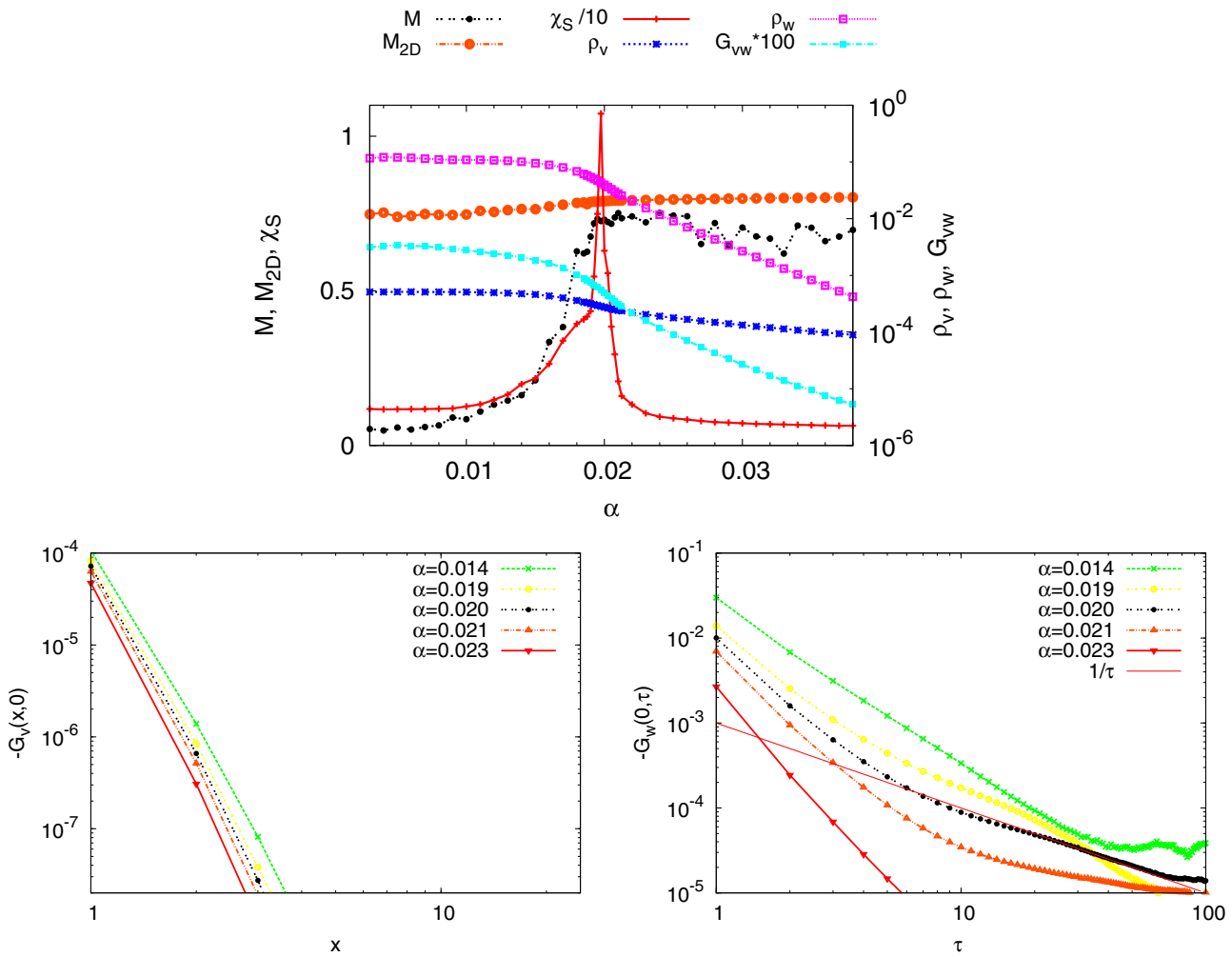

FIG. 5. (Color online) Static properties (top panel), vortex and warp correlation functions (bottom panels) of transition from the quasiordered to the ordered phase. Here, $K_\tau = 0.01$, $K = 1.5$, and α is varied. The results shown are for $N = 50$ and $N_\tau = 200$.

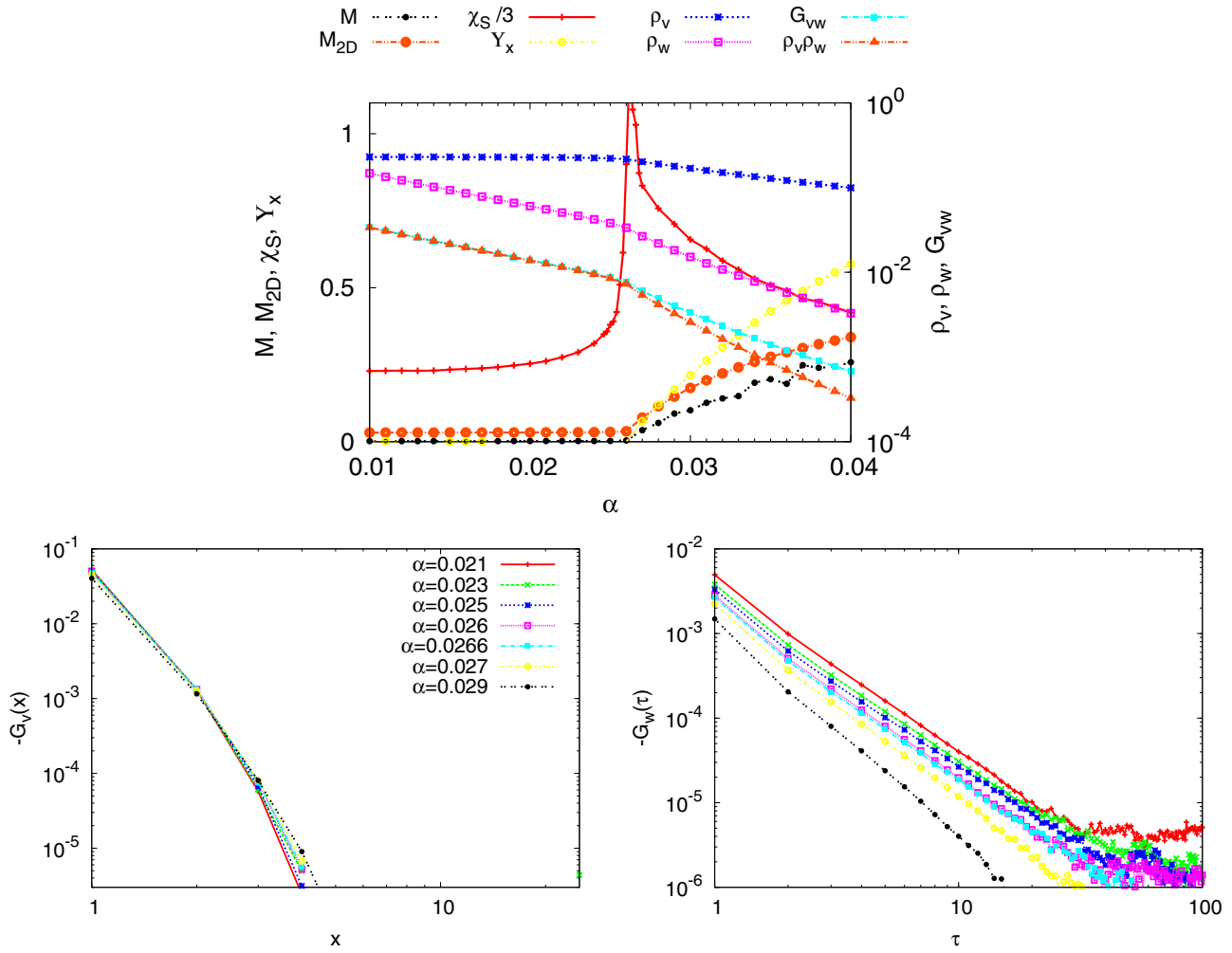

FIG. 6. (Color online) Static properties (top panel), vortex and warp correlation functions (bottom panels) of transition from the disordered to the ordered phase. Here, $K_\tau = 0.01$, $K = 0.4$, and α is varied. The results shown are for $N = 50$ and $N_\tau = 200$. We find that when M_{2D} becomes finite, M varies with the size and only approaches M_{2D} at large system size (see Fig. 3). The vortex and warp correlations are discussed in the text.

in α_c, due to finite-size effects. The helicity modulus Υ_x and magnetization m become finite for $\alpha > \alpha_c$. We notice that both the vortex and the warp densities change slope across α_c. So long-range order appears to develop simultaneously along both the spatial and the temporal directions. However, on the disordered side, the warp density decreases by an order of magnitude as the transition is approached while the vortex density remains unchanged. This indicates a large critical region in which the temporal correlations are expected to grow while the spatial correlations remain short range. On the ordered side, for $\alpha > \alpha_c$, the warp density has a more rapid change than the vortex density. We also plot $\rho_v \rho_w$ explicitly to be compared with the mutual correlation between vortices and warps G_{vw}. We observe that $G_{vw} \propto \rho_w$ and $G_{vw} > \rho_v \rho_w$ when $\alpha > \alpha_c$, i.e., suggesting coupling of vortices to warps inside the ordered phase, while their difference $G_{vw} - \rho_v \rho_w$ vanishes at the critical point and becomes invisible on the disordered side. The study of correlation functions following will show that the spatial correlations do develop on the disordered side but with an exponentially slower dependence on $(\alpha_c - \alpha)$ than the temporal dependencies. These facts suggest that the transition is driven by the quantum freezing of warps. We speculate that this occurs through the third term in the action (8), which drives the fugacity of the vortices so that they also freeze.

The self-correlation functions of vortices and warps are also shown in Fig. 6. The vortex correlation functions are relatively unchanged as α changes across the transition compared to the warp correlation functions, which have similar changes as in the quasiordered phase to the ordered phase transition. Near α_c, the latter shows slower decay at long times. However, whether it has the $1/\tau$ behavior requires a calculation with larger time slices and more iterations to demonstrate.

B. Size dependence of Υ_x and M

We have also studied the difference of the vortex freezing across the disordered to ordered phase transition compared to that across the disordered to quasiordered phase transition (which is of the pure KT type) by contrasting the scaling behavior of the helicity modulus Υ_x at the transitions. We perform a finite-size scaling analysis on Υ_x and the order parameter M, and compare their behaviors with those in

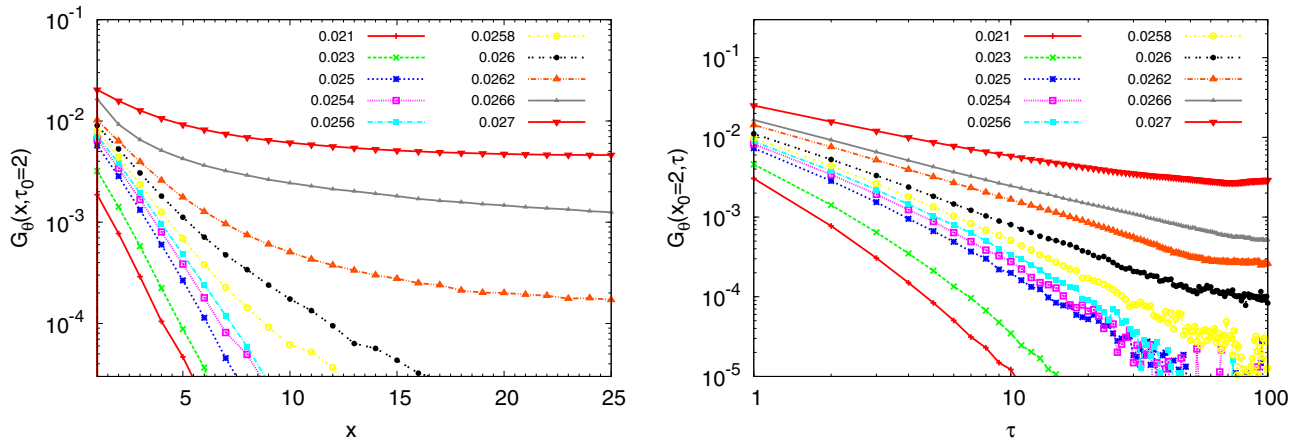

FIG. 7. (Color online) The order-parameter correlation functions $G_\theta(x,\tau)$ for transition from the disordered to the ordered phase. Parameters are the same as in Fig. 6. We show $G_\theta(x,\tau)$ as a function of x for fixed $\tau = 2$ (left panel) and as a function of τ for fixed $x = 2$.

KT transition. The results for two sets of parameters in the quasiordered and the ordered phases have been shown in Fig. 3.

In the classical XY model, the helicity modulus scales with the finite size N of the system as

$$\Upsilon_x(N) = \Upsilon_x(\infty)\left(1 + \frac{1}{2}\frac{1}{\ln N + C}\right), \tag{21}$$

where C is an undetermined constant [31]. At the KT transition point $K = K_c$, the helicity modulus has a jump $\Upsilon_x(\infty)K_c = 2/\pi$. Both the finite-size scaling and the value at the jump have been verified [24] at the disordered to the quasiordered transition. The behavior is quite different in the ordered phase. The stiffness $\Upsilon_x(N)$ in this transition already develops for $\alpha > \alpha_c$ at small sizes and remains unchanged with N. For $\alpha < \alpha_c$, $\Upsilon_x(N)$ decreases exponentially.

The magnetization in the quasiordered KT phase is 0 in the limit $N \to \infty$. But, the passage to this limit is very slow [29]. The finite-size scaling is quite different at the ordered state as shown in Fig. 3. While M_{2D} decreases with N at small N, it is consistent with saturation at a finite value at large N, merging with the value of M. As discussed immediately after the definition of M and M_{2D} above, this is consistent with a truly ordered state.

C. Scaling of the order-parameter correlation functions

The most revealing results about the critical properties are of course obtained from the order-parameter correlation functions. It is seen in Fig. 7 that there exists a separatrix in $G_\theta(x,\tau)$ for a fixed x or for a fixed τ such that, for $\alpha < \alpha_c$ the asymptotic correlation $\to 0$ for large τ, and for $\alpha > \alpha_c$, they tend to a constant value depending on α. We present scaling analysis of the order-parameter correlation functions on the disordered side.

We find that the leading asymptotic behaviors of $G_\theta(x,\tau)$ can be captured in the scaling form

$$G_\theta(x,\tau) = \frac{A}{\tau^{1+\eta_\tau}} e^{-(\tau/\xi_\tau)^{1/2}} \frac{1}{x^{\eta_x}} e^{-x/\xi_x}, \tag{22}$$

where ξ_τ (ξ_x) are correlation lengths along temporal (spatial) directions, and A is the amplitude. From the detailed results given in Appendix A, we determine that the anomalous exponent $\eta_\tau \approx 0$. We cannot determine the anomalous exponent η_x reliably in the numerical calculations because even close to the critical point, where the temporal dependence fits the $1/\tau$ behavior, the spatial dependence continues to be exponentially decreasing as a function of x up to more than $\frac{1}{2}$ the largest sizes that we can numerically calculate (please see Fig. 7). Above that range, it appears to approach a constant, but could be consistent with a logarithmic ($\eta_x = 0$) form. Some discussion of this issue is given in the concluding section.

The correlation functions are shown for a few fixed x as functions of τ in the left panel of Fig. 8 and for a few fixed τ as functions of x in the right panel of the same figure. Fitting the correlation functions to the scaling form in Eq. (22), we determine ξ_x and ξ_τ for each α. We show them as functions of $\alpha - \alpha_c$ in Fig. 9. More details are provided in Appendix A. In the fluctuation regime not too close to the critical point in the disordered side, for $(\alpha_c - \alpha)/\alpha_c \gtrsim 0.1$ with $\alpha_c \approx 0.0260$, we observe that in the parameter range shown, ξ_τ increases by a decade when $\alpha \to \alpha_c$ while ξ_x remains relatively unchanged $\xi_x \approx \xi_{0,x} \approx 1.0$, i.e, a lattice constant. In this range of α, the behavior of ξ_τ is consistent with

$$\xi_\tau(\alpha - \alpha_c) = \tau_c e^{a\sqrt{\alpha_c/(\alpha_c - \alpha)}}, \tag{23}$$

where a is a constant of $O(1)$. This relation, as well as the leading behavior of the correlation function $G_\theta(x,\tau)$,

$$G_\theta(x,\tau) \approx \left(\frac{\tau_c}{\tau}\right) e^{-(\tau/\xi_\tau)^{1/2}} \ln\left(\frac{x_c}{x}\right) e^{-x/\xi_{0,x}}, \tag{24}$$

are identical to those derived analytically [6] (the dependence on ξ_τ, $e^{-(\tau/\xi_\tau)^{1/2}}$, has not been derived explicitly). τ_c is the short-time cutoff scale. It was also derived that, within factors of $O(1)$, $\tau_c = (1/\sqrt{K_0 E_c})/\Delta\tau = 1/\sqrt{K/K_\tau}$. For the parameters chosen, $1/\sqrt{K/K_\tau} = 0.16$, while the numerically obtained value is $\tau_c \approx 0.12$.

However, for $(\alpha - \alpha_c)/\alpha_c \lesssim 0.1$ on the disordered side, there are deviations from Eqs. (23) and (24). For example, we notice in Fig. 7 a crossover from an exponential to a power-law behavior in the spatial correlation as $\alpha \to \alpha_c$ before going to a constant value on the ordered side, consistent with true long-range order. As shown in the left panel of Fig. 9, ξ_x also increases when $\alpha \to \alpha_c$, though at a much slower rate

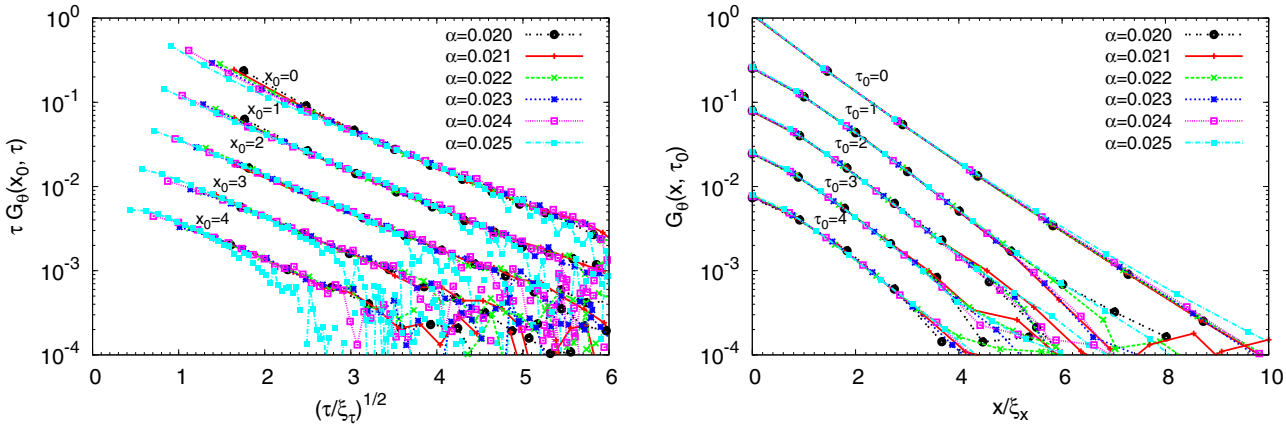

FIG. 8. (Color online) Scaling analysis of the order-parameter correlation function $G_\theta(x,\tau)$ for fixed $x = x_0$ (left panel) and for fixed $\tau = \tau_0$ (right panel) from the disordered side of the disordered to ordered phase transition as shown in Fig. 7. In the left panel, we fit each curve of $\tau G_\theta(x_0,\tau)$ with the form $A_\tau(x)\exp[-(\tau/\xi_\tau)^{1/2}]$, where the amplitude A_τ and the correlation length ξ_τ are fitting parameters adjusted for each α and x. In the right panel, we fit each curve of $G_\theta(x,\tau_0)$ with $A_x(\tau)\exp(-x/\xi_x)$ where $A_x(\tau)$ and ξ_x are fitting parameters. The results of $\xi_\tau(x_0,\alpha)$ and $\xi_x(\tau_0,\alpha)$ are shown in Fig. 9. We find that $A_\tau \approx \tau_c \exp(-x/\xi_{0,x})$ with $\tau_c \approx 0.12$ and $\xi_{0,x} \approx 1.0$, and $A_x \approx (\tau_c/\tau)\exp\{-[\tau/\xi_\tau(\alpha-\alpha_c)]^{1/2}\}$ with $\xi_\tau(\alpha-\alpha_c)$ given in Eq. (23). It is expected that all curves of $\tau G_\theta(x_0,\tau)/A_\tau$ for difference α and x_0 collapse into a single curve $\exp(-t)$ with $t = (\tau/\xi_\tau)^{1/2}$, which are plotted (for clarity, they are rescaled by a factor $10^{(x_0/2)}$ for different x_0). $G_\theta(x,\tau_0)/A_x$ as functions of x/ξ_x are plotted in the same fashion. Because of the rapid decay of the correlation function in this range of α, it has not been numerically possible to follow its behavior for larger x and τ.

compared to ξ_τ. Their monotonic growth suggests scaling one with respect to the other. In the right panel of the same figure, we show that within our numerical capabilities that

$$\xi_x/\xi_{0,x} \approx \ln(\xi_\tau/\tau_c), \tag{25}$$

i.e, the spatial correlation length is consistent with growing as the logarithm of the temporal correlation length. This means that the dynamical critical exponent is $z = \infty$. One should expect, as is consistent with Fig. 9, transients for $x \lesssim \xi_x$ and $\tau \lesssim \xi_\tau$ approaching the forms given above. In Appendix B, we show that within the numerical precision of our results, the relation $\xi_x \propto \xi_\tau^{1/8}$, rather than the logarithmic relation is allowed. Exponents larger than $\frac{1}{8}$ or $z < 8$ are disfavored.

These properties, as well as what has been calculated above about the vortices, appear to be consistent with the suggestion [6] that when warps begin to freeze, spin waves might develop a gap so that the vortices also order (however, this has not been explicitly derived). The approximate correlation function (24) is a separable function of space and time, and so is the final form of the correlation function (22). However, a weak τ dependence $\propto \ln(\tau/\tau_c)$ cannot be excluded in ξ_x very close to criticality. This question can only be settled by further analytical calculations, possibly by a proper renormalization group calculation of the effect of the last term in Eq. (8).

It is worth summarizing the reasons for our suggestion that the freezing of warps drives the (much slower) freezing of vortices: (a) The warp density in Fig. 6 changes by an

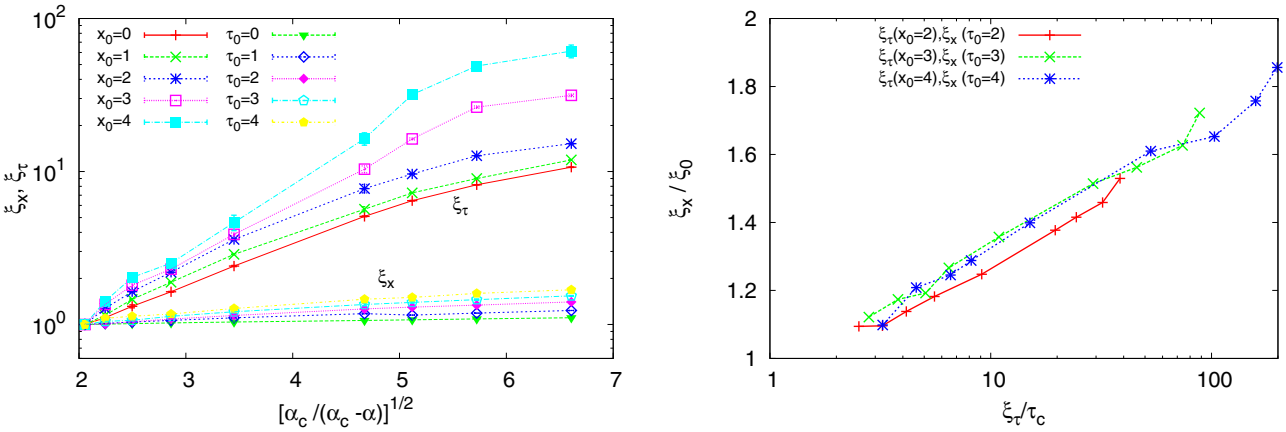

FIG. 9. (Color online) The left panel shows ξ_x and ξ_τ as functions of $[\alpha_c/(\alpha_c-\alpha)]^{1/2}$. They have been rescaled to their respective values at $\alpha = 0.020$ $\{[\alpha_c/(\alpha_c-\alpha)]^{1/2} \approx 2\}$. The error bar is typically smaller than the symbol size; it increases for large ξ_x, i.e., closer to the critical point (note the logarithmic scale). For $x_0 = 0$, ξ_τ can be fitted as $\tau_c \exp[0.62\sqrt{\alpha_c/(\alpha_c-\alpha)}]$; the numerical coefficient in the exponent changes to about 1 for $x_0 = 4$. The right panel shows the relation between $\xi_x(\alpha)$ and $\xi_\tau(\alpha)$. We find that $\xi_x/\xi_0 \sim \ln(\xi_\tau/\tau_c)$. This relation appears to become independent of x and τ at large x and τ. Finite-size effects do not permit a detailed exploration beyond $\xi_\tau/\tau_c \approx 70$.

order of magnitude before there is a discernible change in the density of vortices. (b) The temporal correlation length ξ_τ grows by an order of magnitude as $\alpha \to \alpha_c$ before one notices any change in ξ_r. (c) The disordered to ordered transition is essentially continuous with the quasidisordered to ordered transition which is (vortices having already frozen) driven by the freezing of warps. To notice this in Fig. 2, it should be noted that the figure is drawn with an extremely fine scale of α variation compared to that of K. (d) The exact transformation in terms of warps and vortices from the starting model suggests a renormalization of the parameters for a transition driven by vortices through the variation of fugacity of the warps near their freezing.

From the results here as well as from Ref. [6], the phenomenological expression [8] for quantum-critical fluctuations acquires a crossover towards purely quantum fluctuations below a crossover temperature $T_x \approx \xi_\tau^{-1}$. This presents an essential singularity at the critical point in terms of the tuning parameter of the transition $\alpha - \alpha_c(K, K_\tau)$.

We have presented results for the correlation lengths as a function of $(\alpha - \alpha_c)$. As is evident from the phase diagram, α_c depends on K, and (not explored in this paper) on K_τ, as well. Away from the meeting point of the three transitions, α_c depends smoothly on K. Therefore, we should expect that for fixed α, the change of correlation length is the same function of $(K - K_c)$ as it is of $(\alpha - \alpha_c)$ for a fixed K. However, this point could benefit from further study.

We provide here the form of the correlation functions in frequency-momentum space (assuming $\eta_\tau = \eta_x = 0$) which is convenient to compare with experiments as well as to calculate scattering of fermions from such fluctuation. The Fourier transform from the imaginary-time dependence to real frequency is described in Appendix C, where we show that the final result can only be obtained numerically. We find that the numerical results can be approximately fitted by the form

$$\mathrm{Im}G_\theta(q,\omega) \approx G_0 \frac{1}{q^2 + \kappa_x^2} \rho(\omega, T, \kappa_\tau), \tag{26}$$

$$\rho(\omega, T, \kappa_\tau) \to \frac{\omega}{2\sqrt{T^2 + 0.4\kappa_\tau^2}}, \quad \text{for } \omega/T \to 0$$

$$\to \frac{1}{4}\left(1 + 3e^{-[\kappa_\tau/(2T)]^{1/2}}\right), \quad \text{for } \omega/T \gg 1. \tag{27}$$

Here, $\kappa_x = \xi_x^{-1}(\alpha, K, K_\tau)$, $\kappa_\tau = \xi_\tau^{-1}(\alpha, K, K_\tau)$, and G_0 measures the integrated strength of the fluctuations. The following features of $\mathrm{Im}G_\theta(q,\omega)$ are especially noteworthy. (i) It is a separable function of q and ω. (ii) In the critical region, i.e., $T/\kappa_\tau \gg 1$, $\rho \propto \tanh(\frac{\omega}{2T})$. It should be noted that κ_τ is such a slow function of $(\alpha - \alpha_c)/\alpha_c$ [see Eq. (23)] that the quantum-critical region may be visible over a very wide region of parameters on the disordered side. (iii) The low-frequency part is cut off for $T/\kappa_\tau \ll 1$ with κ_τ replacing T. (iv) For large ω/T, there is a rapid decrease of the correlation function with κ_τ/T. Ultimately, there is an ultraviolet cutoff of the frequency $\omega_c = \tau_c^{-1}$. In any given experimental systems, there may be cutoffs not included in the XY model, for example, the Fermi energy in itinerant Fermion systems.

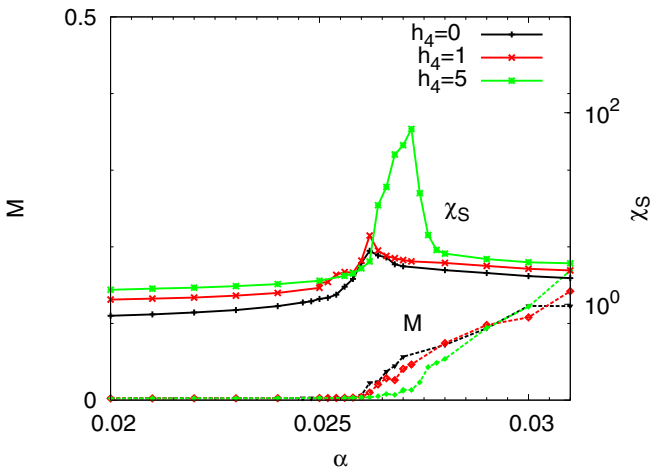

FIG. 10. (Color online) χ_S and M for different h_4. Here, $K = 0.4$, $K_\tau = 0.01$, and α is varied. The system size is kept the same, $N = 50$ and $N_\tau = 200$.

VII. EFFECT OF FOURFOLD ANISOTROPY

We now turn on the fourfold anisotropic field h_4 in the Monte Carlo simulation to study its effect. In the classical XY model, fourfold anisotropy is marginally irrelevant [26]. In the quantum model, it has been argued [6] to be irrelevant. When $h_4 \to \infty$, XY spins become two Ising variables, as in the Ashkin-Teller model. We focus on the transition from the disordered to the ordered phase, by choosing $K = 0.4$, $K_\tau = 0.01$, and tuning α for transitions for different h_4. We find that the transition persists and all quantities have similar properties across the transition as in the $h_4 = 0$ case. In Fig. 10, we compare χ_S and M for three different values of $h_4 = 0, 1, 5$. We find that up to $h_4 = 1$, the properties are almost the same as in $h_4 = 0$. In $h_4 = 5$, we notice that α_c has been shifted to 0.0272, and the peak in χ_S is sharper. M increases more rapidly.

We further show the scaling results of the spin correlation functions for $h_4 = 5$ in Fig. 11. We find similar behaviors as in the $h_4 = 0$ case, which indicates that the transition is also of the local critical type.

VIII. DISCUSSION

In this paper, the properties of the dissipative quantum XY model have been investigated by Monte Carlo simulations to verify and extend the analytical calculations in Ref. [6] and the previous Monte Carlo simulations in Ref. [24]. At criticality, we have found properties consistent with the scaling in ω/T, precisely of the form proposed in Ref. [8] and derived in Ref. [6] with a crossover in time/temperature to the disordered quantum state. We have also found some important results not obtained before that, at criticality, the spatial correlation length also diverges. To our numerical accuracy, the temporal and spatial correlations near criticality are separable. The spatial correlation length varies very slowly, consistent logarithmically with the temporal correlation length. Therefore, the dynamical critical exponent $z = \infty$. It is hoped that this result can also be derived analytically, as also the anomalous exponent η_x. It can be shown, using the separability of the

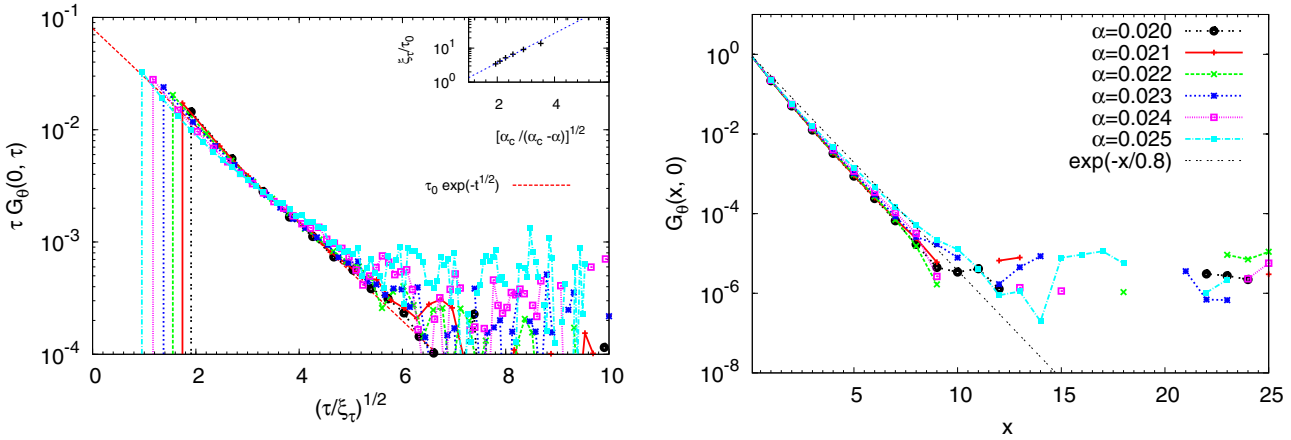

FIG. 11. (Color online) Order-parameter correlation functions for $h_4 = 5$. The left panel shows scaling analysis of the $\mathbf{x} = 0$ spin correlation function $G_\theta(0,\tau)$ from the disordered side of the transition. The fitting curve is similar to that in $h_4 = 0$ case, $G_\theta(0,\tau) = (\tau_0/\tau)\exp[-\sqrt{\tau/\xi_\tau}]$ with $\tau_0 \approx 0.08$. The inset shows ξ_τ/τ_0 as a function of $\sqrt{\alpha_c/(\alpha_c-\alpha)}$. One finds that $\xi_\tau(\alpha)/\tau_0 \approx 0.5\exp[\sqrt{\alpha_c/(\alpha_c-\alpha)}]$, with $\alpha_c = 0.0272$. The right panel shows equal-time spin correlation functions $G_\theta(x,0)$ as functions of x. For $x \lesssim 10$, they have also the same form as in $h_4 = 0$ case $G_\theta(x,0) = \exp(-x/\xi_x)$ with $\xi_x \approx 0.8$.

spatial and temporal correlations and the scaling in ω/T, that scattering of fermions scattering from such fluctuations leads to marginal Fermi-liquid [8] properties.

We reemphasize that the conclusions based on numerical results at finite N and N_τ can at most be highly suggestive. In Appendix B, we show that a dynamical critical exponent of 8 fits the data as well as ∞. The separability of the spatial and temporal dependence of the correlations, which is a feature of the results, depends on the numerical capabilities in which the results are obtained. It is possible that very close to the critical point $(\alpha_c - \alpha)/\alpha_c \lesssim 10^{-2}$, the results could be different. This region is affected by the finite-size or finite-temperature effect, where classical dynamics dominates. Critical slowing down could also be a contributing factor. Such issues are best addressed by analytic methods, to which the present results serve as a guide. However, we can be fairly certain that over the range which is quite close to a critical point, the spatial correlations vary very slowly compared to the temporal correlations and the two are separable, and that the disordered to ordered transition is driven by freezing of the warps with the vortices freezing when the warp correlations become sufficiently long. These results are in the range in which experiments are usually done.

We should also stress that most of the study on the correlation functions is on the disordered side of the quantum-critical point. Some comments may be worthwhile on the ordered side. The ordered side for the problem studied has the properties of the model without dissipation, i.e., it is the ordered phase of the 3D XY type. Some of our preliminary results indicate that as K_τ is increased, the region of the quasiordered phase decreases in the K-α plane. This is in agreement with the fact that when $\alpha \to 0$, the transition as tuned by the ratio of K/K_τ is of the 3D XY type, in which the correlations are expected to be a function of the coordinate $(x^2 + v^2\tau^2)^{1/2}$, where v^2 is given dimensionally in the third term of Eq. (9) by K/K_τ. The results in this paper on the disordered side suggest that v^2 scales near the transition in an interesting way. In the critical region on the disordered side, it vanishes when away from the critical point, indicating that the long-range correlations develop only in time. On the ordered side, it acquires a finite value. We also know that the theory is nonanalytic as $\alpha \to 0$. Properties in the K_τ-α plane are subjects of further study.

It is not the purpose of this paper to discuss the experiments which may be related to the findings here. But, a few comments about future directions in relation to both theory and experiments may be worthwhile.

The dissipative quantum XY model was first proposed [1,2] in connection with the superconductor-to-insulator transition in thin superconducting films [3]. Quite correctly, the transition as a function of dissipation was proven. But, the fluctuation spectra in various calculations [32] in two dimensions were not obtained in a controlled manner and do not agree with the results presented here and in Ref. [6]. (However, the results for the one-dimensional array of Josephson junctions in a dissipative environment [33] are closely related to the results here and in Ref. [6].) Nor do the results of these calculations give the rich phase diagram found in [24] and here, which is suggested by reexpression of the model in terms of warps and vortices. It would be interesting to think of how experiments might discover the different phases in a superconducting thin film. We are also not aware of experiments to probe the fluctuation spectra at the superconductor-to-insulator transitions. This would also be very interesting to pursue, possibly by studying fluctuations across a Josephson junction to a three-dimensional superconductor below its transition temperature. To fully understand such possible experiments, this work should be extended to include (the equivalent of) a magnetic field.

The dissipative quantum XY model (with fourfold anisotropy) has also been proposed [4] as a model for the observed order in the under-doped region of the cuprates. The phenomenological quantum-critical fluctuations, which have been successful in explaining the diverse anomalies in the strange metal region of these compounds, have now been proven to be the property of the fluctuations of the observed

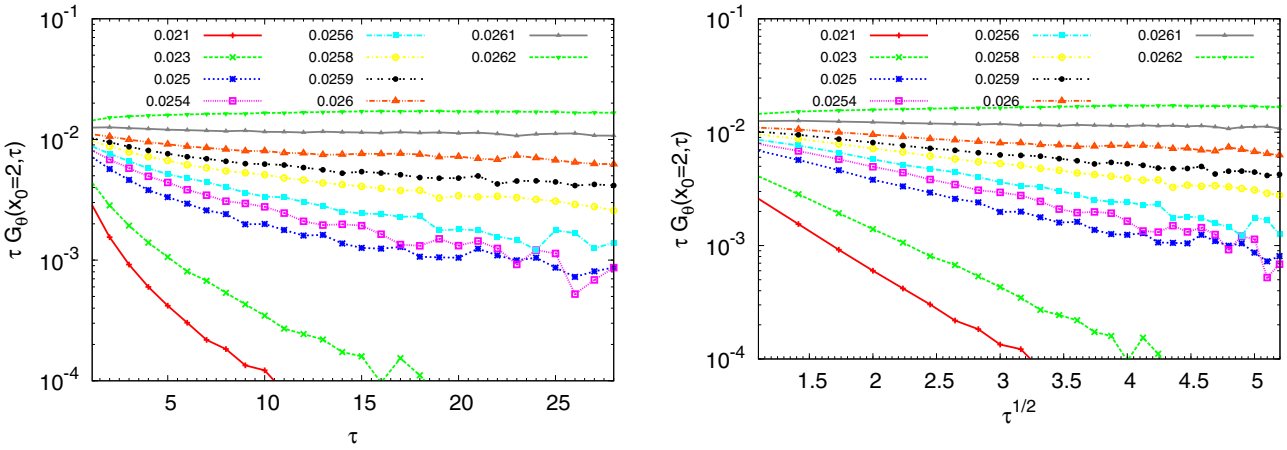

FIG. 12. (Color online) $\ln[\tau G_\theta(x_0 = 2,\tau)]$ as functions of τ (left panel) for selected α's in transition from the disordered to the ordered phase. Other parameters are the same as in Fig. 6. The right panel shows them as functions of $\tau^{1/2}$ instead.

order. It is remarkable that some of the same anomalies observed in the cuprates in this region also occur in the AFM quantum-critical region of some of the heavy fermions and in the Fe-based superconductors. This has led to the inquiry and the conclusion [7] that the criticality of a simple model of itinerant AFM is also described by the dissipative XY model.

ACKNOWLEDGMENTS

We thank A. Sudbø for several conversations and correspondence about the work in Ref. [24], which were very important in this work. We wish to acknowledge very helpful discussions with V. Aji. Some calculations by W. Yan and J. Lou at a preliminary stage of this work are also acknowledged. This work was partly supported by the National Science Foundation under Grant No. NSF-DMR 1206298 (L.Z., C.M.V.), the State Key Programs of China under Grant No. 2012CB921604 (Y.C.), and the National Natural Science Foundation of China under Grant Nos. 11274069, and 11474064 (Y.C.).

APPENDIX A: SCALING FORM OF THE ORDER-PARAMETER CORRELATION FUNCTIONS

We present here results with a much finer variation in α so as to place better bounds on our results. We first discuss the correlations along temporal direction with x fixed at a small value, which take the general scaling form

$$G_\theta(x_0,\tau) \sim \frac{1}{\tau^{1+\eta_\tau}} e^{-(\tau/\xi_\tau)^p}, \tag{A1}$$

where $\xi_\tau \to \infty$ approaching the critical point. In practice, fitting η and p simultaneously leads to uncertainties. The analytical study shows the anomalous scaling dimension for temporal correlation is $\eta_\tau = 0$. Figure 12 shows how the results fit into this form, by plotting $\tau G_\theta(x_0 = 2,\tau)$ as functions of τ. Indeed, we find that near α_c, $\tau G_\theta(x_0 = 2,\tau)$ become almost a constant. Another systematic check is that, very close to α_c and $\tau \ll \xi_\tau$, $G_\theta(x_0,\tau) \sim 1/\tau^\eta$, with only parameter to fit. Fittings to $\alpha = 0.026, 0.0261, 0.0262$ yield $\eta = 1.12 \pm 0.03, 1.03 \pm 0.04, 0.94 \pm 0.03$, respectively. We therefore determine $\eta_\tau \approx 0$. Subsequently, we can decide p. A comparison between fits to the Monte Carlo data with $p = 1$ and $\frac{1}{2}$ is shown in Fig. 12. This shows that $p = \frac{1}{2}$ is much preferred over $p = 1$.

From Fig. 8, it is easy to see the exponential falloff of the spatial correlations characterized by the spatial correlation length ξ_x and determine its dependence on $(\alpha - \alpha_c)$. But, it has proven harder to determine the scaling dimension η_x of the spatial dependence at criticality, as already discussed in the paper.

APPENDIX B: RELATION BETWEEN ξ_x AND ξ_τ: POWER-LAW FITTING

In Fig. 13, we show the relation between ξ_x and ξ_τ could also be fitted as $\xi_x \sim \xi_\tau^{1/8}$, or a dynamic exponent $z \approx 8$. An equally good fit has been shown to a logarithmic form (see Fig. 9). On aesthetic grounds, we may choose the latter.

APPENDIX C: SPECTRAL FUNCTION OF THE ORDER-PARAMETER CORRELATION FUNCTION

The correlation function is in a separable form of τ- and x-dependent terms. Here, we provide the details on Fourier transform from the imaginary-time variable τ to the real-frequency variable ω of the function in Eq. (22), with $\eta_\tau = 0$. A bosonic

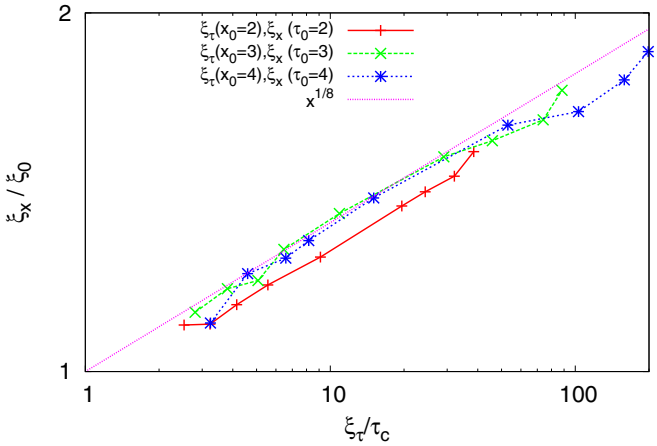

FIG. 13. (Color online) $\xi_x(\alpha;\tau_0)/\xi_0$ as functions of $\xi_\tau(\alpha;x_0)/\tau_c$ in log-log scale.

correlation function in imaginary time $G_b(\tau)$ is related to its spectral function $\rho_b(\omega) = -(1/\pi)\mathrm{Im}G_b(\omega + i0^+)$ by

$$G_b(\tau) = \int_{-\infty}^{\infty} \frac{e^{-\tau\omega}}{1 - e^{-\beta\omega}} \rho_b(\omega) d\omega, \tag{C1}$$

for $0 \leqslant \tau \leqslant \beta$. Setting $t = i(\tau - \beta/2)$, we have

$$G_b(-it + \beta/2) = \int_{-\infty}^{\infty} \frac{e^{it\omega}}{2\sinh(\beta\omega/2)} \rho_b(\omega) d\omega \tag{C2}$$

or

$$\rho_b(\omega) = \frac{\sinh(\beta\omega/2)}{\pi} \int_{-\infty}^{\infty} G_b(-it + \beta/2) e^{-it\omega} d\,t. \tag{C3}$$

We rewrite the time-dependent part of the order-parameter correlation into a periodic form

$$G_\theta(\tau) = \frac{\pi\,\tau_c}{\beta \sin(\pi\,\tau/\beta)} \left(e^{-(\tau/\xi_\tau)^{1/2}} + e^{-[(\beta-\tau)/\xi_\tau]^{1/2}}\right), \tag{C4}$$

which is also particle-hole symmetric $G_\theta(\beta - \tau) = G_\theta(\tau)$, and therefore

$$\begin{aligned} \rho_\theta(\omega) = 2\tau_c \sinh \frac{\beta\omega}{2} \\ \times \int_0^{\infty} \frac{\cos\beta\omega t}{\cosh(\pi\,t)} e^{-(\beta/\xi_\tau)^{1/2}[(1/2)^2+t^2]^{1/4}\cos[(\frac{1}{2}\tan^{-1}2t)]} \\ \times \cos\left\{(\beta/\xi_\tau)^{1/2}[(1/2)^2 + t^2]^{1/4} \right. \\ \left. \times \sin\left(\frac{1}{2}\tan^{-1} 2t\right)\right\} d\,t. \end{aligned} \tag{C5}$$

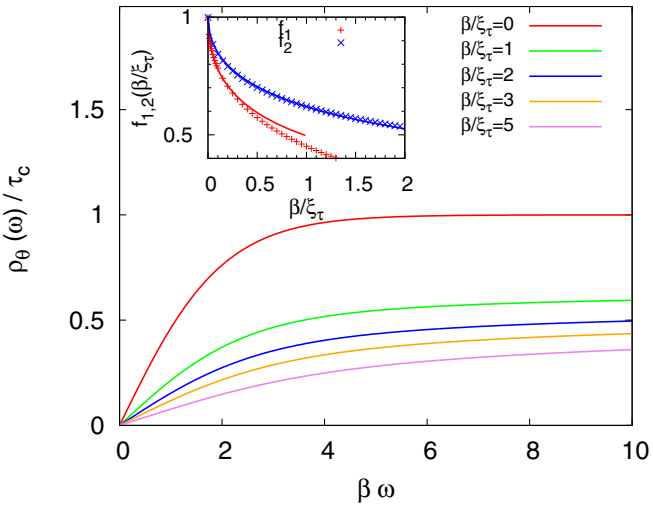

FIG. 14. (Color online) $\rho_\theta(\omega)/\tau_c$ as functions of $\beta\omega$ for selected values of β/ξ_τ. When $\beta\omega \ll 1$, $\rho_\theta(\omega)/\tau_c \to f_1(\beta/\xi_\tau)\beta\omega/2$. When $\beta\omega \gg 1$, $\rho_\theta(\omega)/\tau_c \approx f_2(\beta/\xi_\tau)$. The functions f_1 and f_2 are shown in the inset. Their functional forms in the range of β/ξ_τ shown can be fitted as $f_1(\beta/\xi_\tau) = 1/[1 + 0.42(\beta/\xi_\tau)^{1/2}]^2$ and $f_2(\beta/\xi_\tau) = \frac{1}{4}(1 + 3e^{-[\beta/(2\xi_\tau)]^{1/2}})$, which are shown in solid lines.

This integral can only be evaluated numerically. Results as a function of $\beta\omega$ for several β/ξ_τ are shown in Fig. 14. For $\beta/\xi_\tau \to 0$, $\rho_\theta(\omega) \to \tanh(\beta\omega/2)$, i.e., at finite β/ξ_τ, ξ_τ^{-1} replaces β^{-1} as the infrared cutoff. A different asymptotic form prevails at large $\beta\omega$. The fit to the numerical results is shown in the inset of the figure with analytic forms given in the figure caption and reproduced in Eqs. (26) and (27).

[1] S. Chakravarty, G. L. Ingold, S. Kivelson, and A. Luther, Phys. Rev. Lett. **56**, 2303 (1986).

[2] M. P. A. Fisher, Phys. Rev. Lett. **57**, 885 (1986).

[3] B. G. Orr, H. M. Jaeger, A. M. Goldman, and C. G. Kuper, Phys. Rev. Lett. **56**, 378 (1986); A. F. Hebard and M. A. Paalanen, Phys. Rev. B **30**, 4063 (1984); N. Mason and A. Kapitulnik, Phys. Rev. Lett. **82**, 5341 (1999).

[4] C. M. Varma, Phys. Rev. B **55**, 14554 (1997); **73**, 155113 (2006); M. E. Simon and C. M. Varma, Phys. Rev. Lett. **89**, 247003 (2002).

[5] P. Bourges and Y. Sidis, C. R. Phys. **12**, 461 (2011).

[6] V. Aji and C. M. Varma, Phys. Rev. Lett. **99**, 067003 (2007); Phys. Rev. B **79**, 184501 (2009); **82**, 174501 (2010).

[7] C. M. Varma, arXiv:1502.00577.

[8] C. M. Varma, P. B. Littlewood, S. Schmitt-Rink, E. Abrahams, and A. E. Ruckenstein, Phys. Rev. Lett. **63**, 1996 (1989).

[9] P. C. Hohenberg and B. I. Halperin, Rev. Mod. Phys. **49**, 435 (1977).

[10] M. T. Béal-Monod and Kazumi Maki, Phys. Rev. Lett. **34**, 1461 (1975).

[11] J. A. Hertz, Phys. Rev. B **14**, 1165 (1976).

[12] T. Moriya, *Spin Fluctuations in Itinerant Electron Magnetism* (Springer, Berlin, 1985).

[13] H. v. Löhneysen, A. Rosch, M. Vojta, and P. Wölfle, Rev. Mod. Phys. **79**, 1015 (2007).

[14] R. Zhou, Z. Li, J. Yang, D. L. Sun, C. T. Lin, and G.-q. Zheng, Nat. Commun. **4**, 2265 (2013).

[15] I. M. Hayes, N. P. Breznay, T. Helm, P. Moll, M. Wartenbe, R. D. McDonald, A. Shekhter, and J. G. Analytis, arXiv:1412.6484.

[16] A. Schröder, G. Aeppli, E. Bucher, R. Ramazashvili, and P. Coleman, Phys. Rev. Lett. **80**, 5623 (1998).

[17] A. Schröder, G. Aeppli, R. Coldea, M. Adams, O. Stockert, H. V. Löhneysen, E. Bucher, R. Ramazashvili, and P. Coleman, Nature (London) **407**, 351 (2000).

[18] Q. Si, S. Rabello, K. Ingersent, and J. Lleweilun Smith, Nature (London) **413**, 804 (2001).

[19] In Refs. [16,17], the measured imaginary part of the susceptibility $\chi''(\mathbf{q},\omega)$ at $\mathbf{q} = \mathbf{Q}_0$ has been fit to a local criticality form which has a different form than that derived here. However, we find that there is a very good fit to the measured $\chi''(\mathbf{Q}_0,\omega)$ at different temperatures to $\omega/2T$, for $\omega/2T \lesssim 1$, as derived here. The higher-frequency parts can only be fit by introducing a cutoff $\omega_c \approx 3K$.

[20] V. L. Berezinskii, Zh. Eksp. Teor. Fiz. **59**, 907 (1970) [Sov. Phys. JETP **32**, 493 (1971)].

[21] J. M. Kosterlitz and D. J. Thouless, J. Phys. C: Solid State Phys. **6**, 1181 (1973).

[22] M. P. A. Fisher, G. Grinstein, and S. M. Girvin, Phys. Rev. Lett. **64**, 587 (1990).
[23] This is similar to the classical 3D anisotropic XY model, which shows a 3D to 2D crossover behavior. See, e.g., W. Janke and T. Matsui, Phys. Rev. B **42**, 10673 (1990).
[24] E. B. Stiansen, I. B. Sperstad, and A. Sudbø, Phys. Rev. B **85**, 224531 (2012).
[25] A. O. Caldeira and A. J. Leggett, Ann. Phys. (NY) **149**, 374 (1983).
[26] J. V. José, L. P. Kadanoff, S. Kirkpatrick, and D. R. Nelson, Phys. Rev. B **16**, 1217 (1977).
[27] J. Villain, J. Phys. (Paris) **36**, 581 (1975).
[28] A. M. Polyakov, Nucl. Phys. B **120**, 429 (1977).
[29] S. T. Bramwell and P. C. W. Holdsworth, Phys. Rev. B **49**, 8811 (1994).
[30] D. R. Nelson and J. M. Kosterlitz, Phys. Rev. Lett. **39**, 1201 (1977).
[31] H. Weber and P. Minnhagen, Phys. Rev. B **37**, 5986 (1988).
[32] S. Chakravarty, G. L. Ingold, S. Kivelson, and G. Zimanyi, Phys. Rev. B **37**, 3283 (1988); S. Tewari, J. Toner and S. Chakravarty, *ibid.* **72**, 060505(R) (2005); N. Nagaosa, *Quantum Field Theory in Condensed Matter Physics* (Springer, New York, 1999), Sec. 5.2.
[33] G. Refael, E. Demler, Y. Oreg, and D. S. Fisher, Phys. Rev. B **75**, 014522 (2007).